ChemPubSoc Europe

DOI: 10.1002/chem.201801236

CHEMISTRY A European Journal Full Paper

Coordination Modes | *Hot Paper*

Behavior of Ru–bda Water-Oxidation Catalysts in Low Oxidation States**

Roc Matheu,[a] Abolfazl Ghaderian,[a] Laia Francàs,[a] Petko Chernev,[b] Mehmed Z. Ertem,[c] Jordi Benet-Buchholz,[a] Victor S. Batista,*[d] Michael Haumann,[b] Carolina Gimbert-Suriñach,*[a] Xavier Sala,*[e] and Antoni Llobet*[a, e]

Abstract: The Ru complex $[Ru^{II}(bda\text{-}\kappa\text{-}N^2O^2)(N\text{-}NH_2)_2]$ (**1**; bda^{2-} = 2,2′-bipyridine-6,6′-dicarboxylate, N-NH_2 = 4-(pyridin-4-yl)aniline) was used as a synthetic intermediate to prepare new Ru^{II} and Ru^{III} bda complexes that contain NO^+, MeCN, or H_2O ligands. In acidic solution complex **1** reacts with an excess of NO^+ (generated in situ from sodium nitrite) to form a new Ru complex in which the aryl amine ligand N–NH_2 is transformed into a diazonium salt [N-N_2^+ = 4-(pyridin-4-yl)benzenediazonium)] together with the formation of a new Ru(NO) moiety in the equatorial zone, to generate $[Ru^{II}(bda\text{-}\kappa\text{-}N^2O)(NO)(N\text{-}N_2)_2]^{3+}$ (**2**$^{3+}$). Here the bda^{2-} ligand binds in a κ-N^2O tridentate manner with a dangling carboxylate group. Similarly, complex **1** can also react with a coordinating solvent, such as MeCN, at room temperature to give $[Ru^{II}(bda\text{-}\kappa\text{-}N^2O)(MeCN)(N\text{-}NH_2)_2]$ (**3**). In acidic aqueous solutions, a related reaction occurs in which solvent water coordinates to the Ru center to form $\{[Ru^{II}\{bda\text{-}\kappa\text{-}(NO)^3\}(H_2O)(N\text{-}NH_3)_2](H_2O)_n\}^{2+}$ (**4**$^{2+}$) and is strongly hydrogen-bonded with additional water molecules in the second coordination sphere. Furthermore, under acidic conditions the aniline ligands are also protonated to form the corresponding anilinium cationic ligands N-NH_3^+. Additionally, the one-electron oxidized complex $\{[Ru^{III}\{bda\text{-}\kappa\text{-}(NO)^{3.5}\}(H_2O)(N\text{-}NH_3)_2](H_2O)_n\}^{3+}$ (**5**$^{3+}$) was characterized, in which the fractional value in the κ notation indicates the presence of an additional contact to the pseudo-octahedral geometry of the Ru center. The coordination modes of the complexes were studied in the solid state and in solution through single-crystal XRD, X-ray absorption spectroscopy, variable-temperature NMR spectroscopy, and DFT calculations. While κ-N^2O is the main coordination mode for **2**$^{3+}$ and **3**, an equilibrium that involves isomers with κ-N^2O and κ-NO^2 coordination modes and neighboring hydrogen-bonded water molecules is observed for **4**$^{2+}$ and **5**$^{3+}$.

Introduction

The field of water-oxidation catalysis by molecular transition metal complexes has evolved enormously since the early work of Meyer and co-workers on the blue dimer[1] in the early 1980s.[2] Extremely rugged molecular water-oxidation catalysts (WOCs) based on Ru complexes with turnover numbers (TONs) in some cases greater than 10^6 have been recently reported with confirmed molecular structure maintained throughout the entire catalytic process.[3–5] A prominent family of these catalysts are the recently reported Ru complexes based on the tetradentate ligand 2,2′-bipyridine-6,6′-dicarboxylate (bda^{2-}; see Scheme 1 for formulas of all ligands described in this work).[6–10] In some cases these complexes have catalytic activity that is comparable to that of the natural oxygen-evolving complex of photosystem II (OEC-PSII) in green plants and algae.[11,12] Further, even more active catalysts containing a related pentadentate ligand, such as 2,2′:6′,2″-terpyridine-6,6″-dicarboxylate (tda), have been reported recently.[13,14]

The Ru-bda complexes of general formula $[Ru(bda)(N\text{-}Ax)_2]$ (N-Ax is a neutral monodentate pyridyl-type ligand in axial position) constitute a family of complexes that are easy to prepare and whose properties can be tuned through the axial ligand. Indeed, the different natures of the axial ligands can

[a] *R. Matheu, A. Ghaderian, L. Francàs, J. Benet-Buchholz, C. Gimbert-Suriñach, A. Llobet*
Institute of Chemical Research of Catalonia (ICIQ)
Barcelona Institute of Science and Technology (BIST)
Avinguda Països Catalans 16, 43007 Tarragona (Spain)
E-mail: cgimbert@iciq.es
allobet@iciq.es

[b] *P. Chernev, M. Haumann*
Institute for Experimental Physics, Free University Berlin
14195 Berlin (Germany)

[c] *M. Z. Ertem*
Chemistry Department, Brookhaven National Laboratory
Upton, NY 11973 (USA)

[d] *V. S. Batista*
Department of Chemistry, Yale University
P.O. Box 208107, New Haven, CT 06520-8107 (USA)
E-mail: victor.batista@yale.edu

[e] *X. Sala, A. Llobet*
Departament de Química, Universitat Autònoma de Barcelona
Cerdanyola del Vallès, 08193 Barcelona (Spain)
E-mail: xavier.sala@uab.cat

[**] *bda: 2,2′-bipyridine-6,6′-dicarboxylate.*

Supporting information (synthetic procedures, X-ray crystallographic data in CIF format; additional experimental, spectroscopic, electrochemical, and computational data) and the ORCID identification numbers for the authors of this article can be found under: https://doi.org/10.1002/chem.201801236.

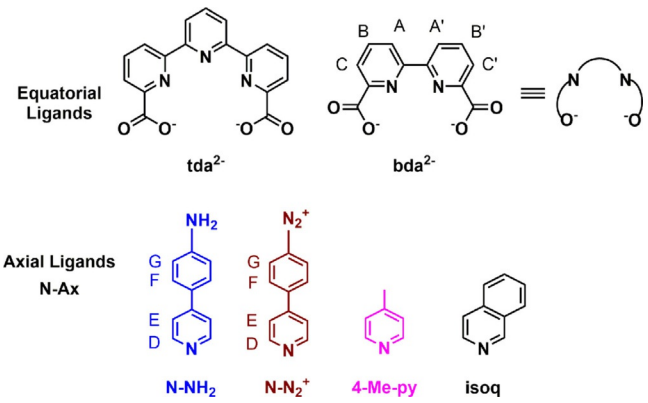

Scheme 1. Ligands used and discussed in this work with labels for NMR assignment.

exert steric, electronic, or supramolecular effects that influence the properties of the catalyst.[2,6,8,15,16] In addition, axial ligands with appropriate functionalities have been used to immobilize this class of complexes on conducting solid surfaces.[17–21]

In oxidation state II the [Ru(bda)(N-Ax)$_2$] complexes have a saturated coordination sphere with distorted octahedral geometry. As such they are not WOCs but in fact catalyst precursors. These complexes enter the catalytic cycle on coordinating a water molecule and reaching higher oxidation states.[6,20,22,23] The Ru-aqua functionality is important since it provides the capacity to lose protons and electrons in a concerted fashion at relatively low potentials and at the same time provides for an O–O bond-formation site. For the particular case in which the axial ligand is 4-methylpyridine (4-Me-py), the X-ray crystal structure of {[[Ru^{IV}(OH)(bda-κ-N^{2}O^2)(4-Me-py)$_2$](H$_2$O)]$_2$(μ-H)}$^{3+}$ revealed a seven-coordinate coordination sphere for the Ru^{IV} center with a pseudo-pentagonal-bipyramidal geometry.[24] In sharp contrast, in oxidation state II, the corresponding Ru-aqua complexes are not well characterized. Interestingly, the coordination geometry of the d^6 Ru^{II} ion is expected to be octahedral, since sevenfold coordination would imply violation of the 18-electron rule.[25] Thus, assuming the axial ligands do not detach from the Ru-aqua complex, as evidenced by ^{1}H NMR spectroscopy,[23] the bda^{2-} ligand must partially decoordinate to generate either a dangling carboxylate group or a frustrated coordination site by decoordination of one of Ru–N bonds of the bipyridyl moiety.[20,23,26] The latter is an interesting concept, recently developed, with implications in a variety of processes including heterolytic H$_2$ splitting.[27,28]

The main goal of the present work was to shed light on the potential coordination modes of the bda^{2-} ligand for low oxidation states (i.e., Ru^{II} and Ru^{III}), which is crucial for the coordination of an aqua ligand that provides entry into the catalytic cycle. For this purpose, we prepared a family of Ru-bda complexes (**1**–**5**$^{3+}$ in Scheme 1) and characterized them by X-ray diffraction, spectroscopic methods, and DFT calculations.

Results and Discussion

Synthesis and solid-state structures

We used [Ru^{II}(bda-κ-N^{2}O^2)(N-NH$_2$)$_2$] (**1**),[17] which has 4-(pyridin-4-yl)aniline (N-NH$_2$) ligands in the axial positions, as the starting material for all the complexes described in this work (Scheme 2). We chose **1** because of its solubility both in certain organic solvents and in acidic water and because the amino functionality gives easy synthetic access to the family of Ru-bda complexes depicted in Scheme 2. This family allows us to obtain a large variety of spectroscopic properties that analyzed together provide a consistent and comprehensive description of the phenomena occurring in Ru-bda complexes in low oxidation states. Further, the remotely located amino groups do not influence significantly the redox potential of the Ru complex.[17]

The solid-state structure of **1** was analyzed by XRD, DFT calculations, and X-ray absorption spectroscopy (XAS). Single crystals of **1** were obtained by slow diffusion of diethyl ether into a methanol solution, and an ORTEP of its structure is shown in Figure 1 and the bond lengths and angles are similar to those of related Ru^{II} complexes containing similar types of ligands ($d_{Ru-O/Ru-N}$ = 1.9–2.1 Å).[24,29–31] The most interesting feature is the equatorial geometry of the first coordination sphere imposed by the bda^{2-} ligand, generating an O-Ru-O angle of 121.7°. XAS at the Ru K-edge was carried out on a powder of **1** (Figure 2). The bond lengths obtained by extended X-ray absorption fine structure (EXAFS) simulation are listed in Table 1 and show very good agreement with the XRD data. Further, DFT calculations were carried out for geometrical optimization of **1** at the M06 level of theory,[32] and the main geometric parameters are also listed in Table 1, while the complete data can be found in the Supporting Information. The high degree of consistency of all the metric parameters obtained for **1** by these three methodologies is noteworthy and gives a high level of confidence when they are used for other related structural characterizations (see below).

Complex **1** reacts with an excess of NO$^+$ (generated in situ from sodium nitrite)[33] in acidic solution to form [Ru^{II}(bda-κ-N^{2}O)(NO)(N-N$_2$)$_2$]$^{3+}$ (**2**$^{3+}$), in which the aryl amine ligands of **1** are transformed into diazonium salts [N-N$_2^+$ = 4-(pyridin-4-yl)-benzenediazonium)]. In addition, a new Ru(NO) moiety is also formed at the equatorial zone according to Equation (1). Addition of a saturated solution of KPF$_6$ allows its isolation as a powdery salt.[17]

$$\underset{\mathbf{1}}{[Ru^{II}(bda\text{-}\kappa\text{-}N^2O^2)(N\text{-}NH_2)_2]} + 3\ NO^+ \longrightarrow \underset{\mathbf{2}^{3+}}{[Ru^{II}(bda\text{-}\kappa\text{-}N^2O)(NO)(N\text{-}N_2)_2]^{3+}} + 2\ H_2O \quad (1)$$

Suitable single crystals for XRD analysis of **2**$^{3+}$ were obtained by slow evaporation of an acidic aqueous solution (see Figure 1 for ORTEP). The nitrosyl ligand occupies one of the equatorial positions and bda^{2-} ligand exhibits a κ-N^{2}O coordination mode. Such a coordination mode releases the geometri-

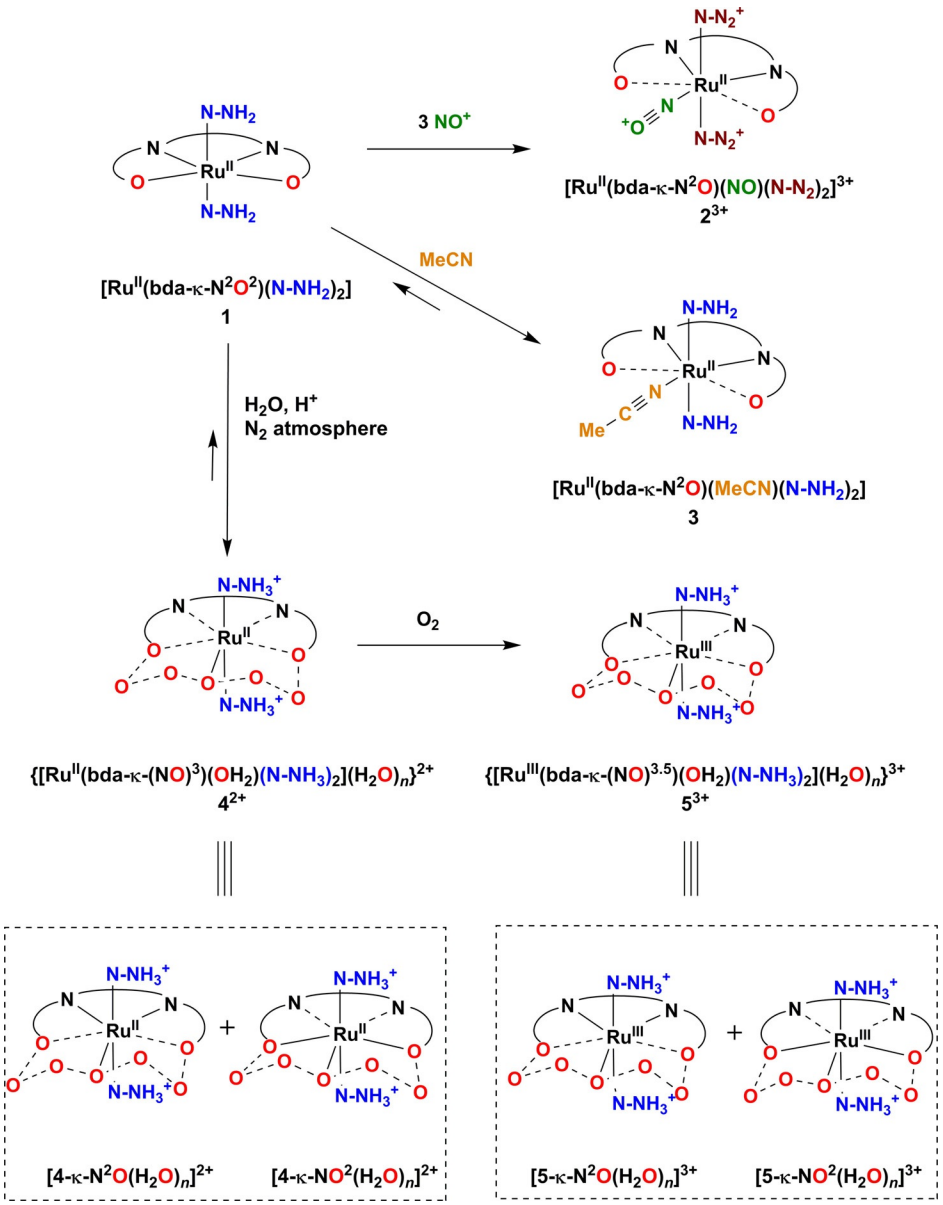

Scheme 2. General synthetic scheme of complexes. The dashed lines in the first coordination sphere of the Ru center indicate bonds that are simultaneously formed and broken. See Scheme 1 for the detailed structures of the axial and equatorial ligands. The dashed lines in $\mathbf{4}^{2+}$ and $\mathbf{5}^{3+}$ in the second coordination sphere represent hydrogen bonding to solvent water molecules.

cal strain in the equatorial plane in **1** and produces a dangling carboxylate group that is not bonded to the Ru center. The κ-N^2O coordination mode is also favored by the crystal packing of the molecule, whereby the dangling carboxylate group interacts with the N atoms of the diazonium groups of another molecule to form dimers (Figure S9 in the Supporting Information). The near linearity of the Ru-N-O^+ unit (175.8°) and the N–O bond length (d_{N-O} = 1.13 Å) indicate N–O triple-bond character. DFT calculations at the M06 level of theory again gave geometric parameters that are very consistent with those obtained by X-ray diffraction (Figure 3, left and Table S2 in the Supporting Information). In particular, $\mathbf{2}^{3+}$ is classified as a closed-shell singlet with a nearly linear Ru-N-O^+ group (174.7°) and d_{N-O} = 1.14 Å confirming the $Ru^{II}(N{\equiv}O^+)$ nature.

Complex **1** can also react with a coordinating solvent at room temperature, for example, with MeCN to give [Ru^{II}(bda-κ-N^2O)(MeCN)(N-NH_2)$_2$] (**3**), as shown in Equation (2). In this complex, the MeCN ligand coordinates to the Ru center in the equatorial plane and again forces the Ru-bda moiety to rearrange its coordination mode by releasing one carboxylate group, similar to what is observed for $\mathbf{2}^{3+}$. Single crystals of **3** were obtained by slow diffusion of diethyl ether into a solution of **1** in MeOH/MeCN (4:1), and its ORTEP is shown in Figure 1. The bda^{2-} ligand coordinates to the Ru center in a κ-N^2O fashion with a pendant carboxylate group, similar to the coordination mode exhibited in $\mathbf{2}^{3+}$. Calculations at the M06 level of theory provided geometrical parameters for **3** analogous to those obtained by XRD (see Table S3 in the Supporting Information).

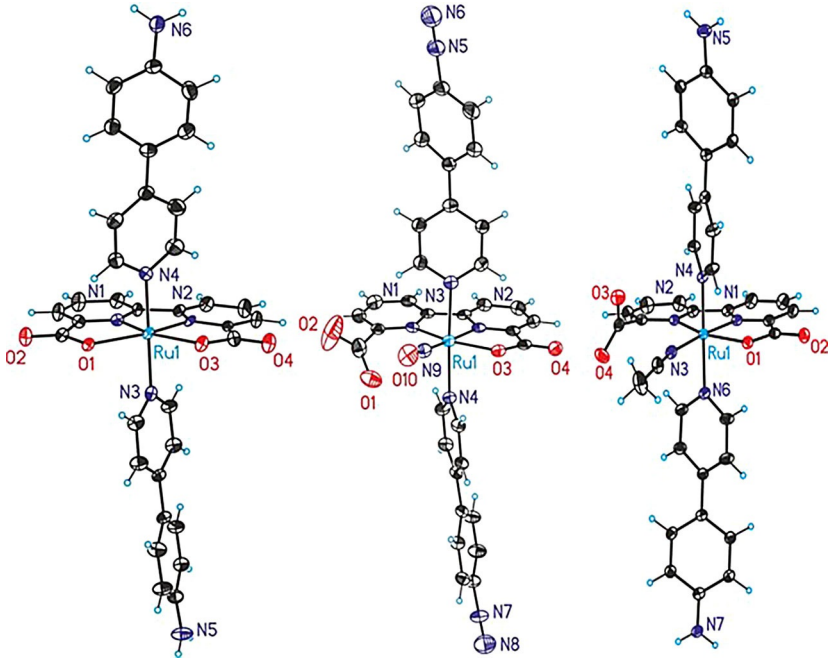

Figure 1. ORTEPs (ellipsoids at 50% probability) and labeling scheme of **1** (left), the cationic part of $\mathbf{2}^{3+}$ (middle), and **3** (right). Color codes: Ru, cyan; N, blue; O, red; C, black; H, light blue.

$$[Ru^{II}(bda\text{-}\kappa\text{-}N^2O^2)(N\text{-}NH_2)_2] + MeCN \rightleftharpoons [Ru^{II}(bda\text{-}\kappa\text{-}N^2O)(MeCN)(N\text{-}NH_2)_2] \quad (2)$$

1 **3**

$$[Ru^{II}(bda\text{-}\kappa\text{-}N^2O^2)(N\text{-}NH_2)_2] + 2\,H^+ + (n+1)\,H_2O \rightleftharpoons \{[Ru^{II}(bda\text{-}\kappa\text{-}(NO)^3)(H_2O)(N\text{-}NH_3)_2](H_2O)_n\}^{2+} \quad (3)$$

1 $\mathbf{4}^{2+}$

The coordination of MeCN is an equilibrium in which the solvent molecule coordinates to and decoordinates from the Ru center. This equilibrium can be controlled by the concentration of MeCN. For instance, the addition of 20% of MeCN to a solution of **1** in methanol allows quantitative generation of **3**, as determined by 1D and 2D NMR spectroscopy (see Figures S1–S7 in the Supporting Information). However, even if the amount of **1** present in equilibrium is negligible, as indicated by NMR spectroscopy, it precipitates from the solution as a powder, probably due to its very low solubility.

At pH 1.0, **1** reacts with the water solvent to form $\{[Ru^{II}\{bda\text{-}\kappa\text{-}(NO)^3\}(H_2O)(N\text{-}NH_3)_2](H_2O)_n\}^{2+}$ [$\mathbf{4}^{2+}$, Eq. (3)]. Again, coordination occurs in the equatorial plane with subsequent change in the coordination mode of the bda^{2-} ligand. In this case, modification of the first coordination sphere involves the presence of a network of strongly hydrogen bonded H_2O molecules as a second coordination sphere. The number of H_2O molecules involved in this network is designated *n*, and they strongly interact with the Ru(aqua) moiety and the carboxylate groups of the bda^{2-} ligand. In addition, at this pH the amino groups are protonated to form the corresponding ammonium salts. The proposed $\mathbf{4}^{2+}$ shows two limit isomeric structures, namely, $[\mathbf{4}\text{-}\kappa\text{-}N^2O(H_2O)_n]^{2+}$ and $[\mathbf{4}\text{-}\kappa\text{-}NO^2(H_2O)_n]^{2+}$, denoted $\kappa\text{-}(NO)^3$, the relative occurrence of which is discussed below. As is observed for **3**, in the solid state the equilibrium shifts towards the more insoluble isomer and generates **1** again with no water coordinated to the metal center.

Finally, $\mathbf{4}^{2+}$ can easily be oxidized by atmospheric oxygen to paramagnetic d^5 Ru^{III} complex $\{[Ru^{III}\{bda\text{-}\kappa\text{-}(NO)^{3.5}\}(H_2O)(N\text{-}NH_3)_2](H_2O)_n\}^{3+}$ ($\mathbf{5}^{3+}$), as shown in Scheme 2. The fractional value in the κ notation here indicates the presence of an additional contact to the pseudo-octahedral geometry of the Ru center that we consistently found for this type of complexes. This oxidation was monitored by UV/Vis spectroscopy and takes place with a $t_{1/2}$ value of approximately 3.3 min at RT according to a first-order mechanism (see Figures S10 and S11 in the Supporting Information). The complex was analyzed in solution by EPR spectroscopy and XAS (see below and Supporting Information).

Dynamic behavior in organic solvents

The solution structures of $\mathbf{2}^{3+}$ and **3** were investigated by variable-temperature (VT) NMR spectroscopy in organic solvents and by DFT calculations, and the spectra are shown in Figure 4 and in Figures S12 and S13 of the Supporting Information. Figure 4 shows the ^1H NMR spectra of $\mathbf{2}^{3+}$ in $[D_6]$acetone in the temperature range 273–193 K. At 273 K the ^1H NMR spectrum of $\mathbf{2}^{3+}$ is not consistent with the $\kappa\text{-}N^2O$ binding mode of the bda^{2-} ligand found in the solid-state X-ray structure. As the temperature is lowered the resonances due to the bda^{2-} ligand broaden, split, and become consistent with the asymmetry observed in the X-ray structure. At 193 K all resonances were unambiguously assigned on the basis of 2D NMR spec-

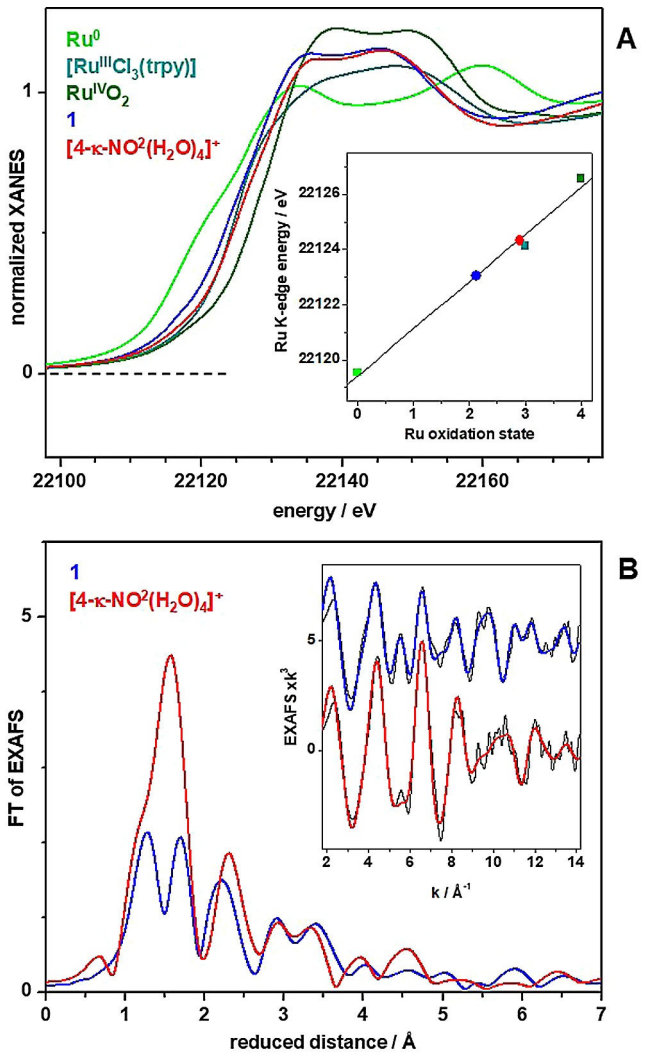

Figure 2. XAS analysis of **1** and $\mathbf{5}^{3+}$. Data for Ru metal, RuO_2, and $[RuCl_3(trpy)]$ are shown for comparison. A) Ru K-edge spectra. Inset: correlation between K-edge energies (determined at 50% edge magnitude) and Ru oxidation states. B) Fourier transforms (FTs) of the EXAFS spectra in the inset. FTs (experimental data) were calculated for *k* values of 1.8–14.2 $Å^{-1}$ and by using $\cos^2$ windows extending over 10% at both *k*-range ends. Spectra are vertically shifted for comparison. Inset: EXAFS oscillations in *k* space (spectra are vertically shifted for comparison). Thin black lines are experimental data, and colored lines are simulations with parameters shown in Table 1 and the Supporting Information.

troscopic data (see Figure S12 in the Supporting Information) and the DFT calculated chemical shifts (see Figure 4). The broadening and splitting of the bda^{2-} resonances at lower temperatures indicates the presence of dynamic behavior in which the two carboxylate groups of the bda^{2-} ligand coordinate and decoordinate very rapidly (Scheme 3). This is further corroborated by the fact that the resonances for protons C and C′ (see Scheme 1) contiguous to the carboxylate group are by far the ones that suffer the largest shift of more than 0.4 ppm. An activation energy of 12.5 kcal mol^{-1} is obtained for this process from the spectra (see Figure S14 in the Supporting Information). We also obtained optimized structures for $Ru^{II}(NO^+)$ complexes by DFT calculations with both κ-N^2O and κ-$(NO)^3$ modes of the bda^{2-} ligand and found the latter binding mode, which is proposed to be the transition state in the interconversion, to be higher in energy by 6.2 kcal mol^{-1} (see Scheme 3 and Figure 3).

Similar behavior is observed for the Ru^{II}(MeCN) complex **3** in [D_3]acetonitrile/[D_4]MeOH (1:4) but with subtle differences (see Figure S13 in the Supporting Information). At RT the main isomer observed is the κ-N^2O, the resonances of which coalesce on heating to a temperature close to 320 K. In this case, the activation energy obtained from the spectra is 15.0 kcal mol^{-1} (see Figure S15 in the Supporting Information).

The X-ray structures and VT NMR results clearly show a preference for the κ-N^2O coordination mode of the bda^{2-} ligand in $\mathbf{2}^{3+}$ and **3**, in the absence of hydrogen bonding with the second coordination sphere. The preference for the κ-N^2O coordination mode for Ru-bda complexes with coordinated MeCN ligand has been observed in related Ru-bda complexes.[34,35] This is in agreement with the HSAB theory,[36] according to which Ru in low oxidation states prefers soft π-acceptor ligands such as pyridyl over hard carboxylate ligands.

Dynamic behavior in acidic aqueous solutions

The ^{1}H NMR spectrum of **1** was recorded in [D_4]MeOH at room temperature and with increasing amounts of a solution with pD = 1.0 (Figure 5). In pure [D_4]MeOH the ^{1}H NMR spectrum of **1** is typical of a six-coordinate Ru^{II} complex with C_{2v} symmetry. All resonances could be unambiguously assigned on the basis of 2D NMR spectra[17] and were also supported by NMR chemical shifts calculated at the M06 level of theory. However, the addition of CF_3SO_3D dissolved in D_2O significantly broadened the resonances, and some of them were strongly shifted (Figure 5). The F protons (Scheme 1), which are close to the amino group, suffer the largest shift due to protonation of the amino group. The small shift of the D protons indicates that the Ru center is almost unaffected by protonation of the amino groups. Further, at 25% of pD = 1.0 solution, we recorded VT NMR spectra up to 240 K, at which the resonances sharpen again, as shown in Figure 5 (right), consistent with the presence of a single symmetrical isomer. In contrast to the previous VT NMR spectra for $\mathbf{2}^{3+}$, now both B and C protons show similar shifts, which suggest a different type of dynamic behavior in which both the Ru–N and Ru–O bonds are simultaneously formed and broken (Scheme 4). Further, the VT NMR results are consistent with coordination of a water molecule to the Ru center on addition of an acidic aqueous solution. The formation and breaking of the Ru^{II}–OH_2 bond occurs simultaneously with a dynamic behavior involving species $\mathbf{[4\text{-}\kappa\text{-}N^2O(H_2O)_n]^{2+}}$ and $\mathbf{[4\text{-}\kappa\text{-}NO^2(H_2O)_n]^{2+}}$, which interconvert through the transition states TS-A, TS-B, and TS-C (Scheme 4). The sharpening of the ^{1}H resonances at low temperature is consistent with the absence of coordination/decoordination of water to/from the Ru center but with all the equilibria indicated in Scheme 4 occurring very fast. In sharp contrast, when **1** is dissolved in neutral aqueous solutions, for example, in [D_4]MeOH/D_2O (4:1), the VT ^{1}H NMR experiments reveal that

Table 1. Metric parameters obtained for **1**, $\mathbf{4}^{2+}$, and $\mathbf{5}^{3+}$ by XRD, EXAFS, and DFT.

	1			$\mathbf{4}^{2+}$			$\mathbf{5}^{3+}$	
Distance[a]	XRD	EXAFS (N)[b]	DFT[c]	DFT[c] $[\mathbf{4}\text{-}\kappa\text{-}NO^2(H_2O)_4]^{2+}$	DFT[c] $[\mathbf{4}\text{-}\kappa\text{-}N^2O(H_2O)_4]^{2+}$	EXAFS (N)[b]	DFT[c] $[\mathbf{5}\text{-}\kappa\text{-}NO^2(H_2O)_4]^{3+}$	DFT[c] $[\mathbf{5}\text{-}\kappa\text{-}N^2O(H_2O)_4]^{3+}$
Ru–OH_2	–	–	–	2.09	2.18	1.92 (1)	2.03	2.13
Ru–NO	–	–	–	–	–	–	–	–
Ru–N1	1.92	1.92 (2)	1.93	**2.82**	1.94	**2.54** (1)	**2.46**	1.99
Ru–N2	1.93	–	1.93	2.26	2.12	2.11 (3)	**2.32**	2.14
Ru–O1	2.16	2.17 (2)	2.17	2.05	2.12	–	2.03	2.05
Ru–O2	2.18	–	2.17	2.23	**3.45**	–	2.08	**3.06**
Ru–N3	2.07	2.07 (2)	2.08	2.04	2.08	2.01 (2)	2.10	2.11
Ru–N4	2.09	–	2.09	2.06	2.11	–	2.10	2.14
ΔG [kcal mol^{-1}]				20.3	0.0		2.1	0.0

[a] The labeling scheme is the same as that used for structure of **1** depicted in Figure 1. All distances in Ångstrom. [b] Distances between the Ru center and the atoms in its first and second coordination spheres. *N* is the coordination number, defined as the number of atoms associated with a particular distance. Additional EXAFS fit parameters (Debye–Waller factors and error sums) are given in Table S1 in the Supporting Information. N and O coordination is indistinguishable in EXAFS analysis, as are the locations of ligands in equatorial or axial positions; therefore, in the table the distances from EXAFS were ordered to comply with the DFT results. [c] M06 functional; see Supporting Information for details. [d] Boldface indicates Ru–N or Ru–O distances relevant to the discussion of κ-NO^2 versus κ-N^2O isomers.

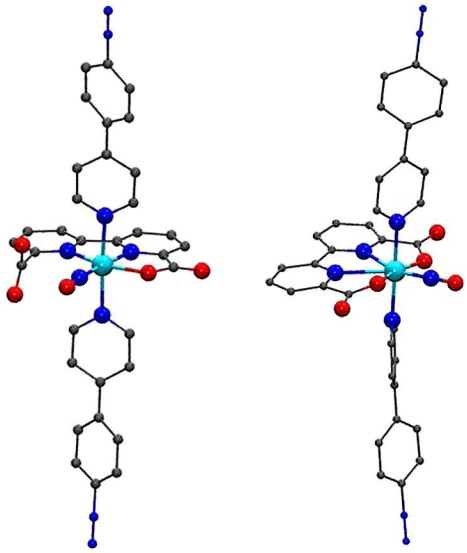

Figure 3. Ball-and-stick representation of the optimized structures at the M06 level of theory for $[\mathbf{2}\text{-}\kappa\text{-}N^2O]^{3+}$ and $[\mathbf{2}\text{-}\kappa\text{-}(NO)^3]^{3+}$ that connects the two limiting structures shown in Scheme 3. Color code: Ru, cyan; C, gray; N, blue; O, red; H atoms of the ligands were omitted for clarity.

the equilibrium involving aqua coordination/decoordination to Ru is still present (Figure S16 in the Supporting Information).

The presence of $[\mathbf{4}\text{-}\kappa\text{-}NO^2(H_2O)_n]^{2+}$ is favored by solvent H_2O molecules strongly hydrogen bonded to the Ru(H_2O) group and the carboxylate moiety of the bda^{2-} ligand. This hydrogen bonding pushes the bipyridyl part of the bda^{2-} ligand away from the metal center and explains why the intuitively preferred Ru–N coordination mode for a soft, low-spin d^6 Ru^{II} ion is not always favored.

All the NMR measurements were performed under strict N_2-atmosphere conditions to avoid oxidation of $\mathbf{4}^{2+}$ to $\mathbf{5}^{3+}$ (see NMR methods in the Supporting Information for further details). To further prove that $\mathbf{4}^{2+}$ remains in oxidation state II, we prepared solutions of $\mathbf{4}^{2+}$ in an identical manner to those prepared for NMR analysis and carried out EPR measurements. The absence of an EPR signal rules out the formation of any traces of the one-electron oxidized species $\mathbf{5}^{3+}$ and thus confirms that the nature of the NMR resonance broadening is solely due to the dynamic behavior. The same behavior also occurs in other Ru-bda catalysts such as [Ru(bda-κ-N^2O^2)(isoq)$_2$] (isoq = isoquinoline) under exactly the same conditions as for **1**, as shown in Figure S18 in the Supporting Information. The comparable shifts and broadening of the resonances observed for the [Ru(bda-κ-N^2O^2)(isoq)$_2$] complex suggests that this is a general phenomenon occurring in Ru-bda complexes.

We carried out DFT calculations for both the $[\mathbf{4}\text{-}\kappa\text{-}NO^2(H_2O)_n]^{2+}$ and $[\mathbf{4}\text{-}\kappa\text{-}N^2O(H_2O)_n]^{2+}$ isomers using either two or four water molecules of solvation. We chose a limited number of water molecules as a model, although clearly a much larger number of water molecules will be involved as second and third coordination spheres of the Ru center. The structures with two or four water molecules of solvation yielded similar results in terms of geometrical features and relative energies of the isomers (see Figures S21 and S22 and Tables S4 and S5 in the Supporting Information). To simplify the discussion we present only $[\mathbf{4}\text{-}\kappa\text{-}NO^2(H_2O)_4]^{2+}$ and $[\mathbf{4}\text{-}\kappa\text{-}N^2O(H_2O)_4]^{2+}$ isomers, the optimized geometries and relevant metric parameters of which are depicted in Figure 6 and Table 1. The first interesting feature of the optimized structures for $[\mathbf{4}\text{-}\kappa\text{-}NO^2(H_2O)_4]^{2+}$ and $[\mathbf{4}\text{-}\kappa\text{-}N^2O(H_2O)_4]^{2+}$ is the presence of a hydrogen-bonding network between the Ru-aqua group and the carboxylate groups of the bda^{2-} ligand which resembles that in the crystal structure of {[[Ru^{IV}(OH)(bda-κ-N^2O^2)(4-Mepy)$_2$](H$_2$O)]$_2$(μ-H)}$^{3+}$.[24] It is also informative to compare the distances between Ru and the N and O atoms of the bda^{2-} ligand in both isomers. For the $[\mathbf{4}\text{-}\kappa\text{-}N^2O(H_2O)_4]^{2+}$ isomer these distances are very similar to those of $\mathbf{2}^{3+}$ with a characteristic distance between the Ru atom and the O atom of the dangling carboxylate group of 3.45 Å. On the other hand, for [**4**-κ-

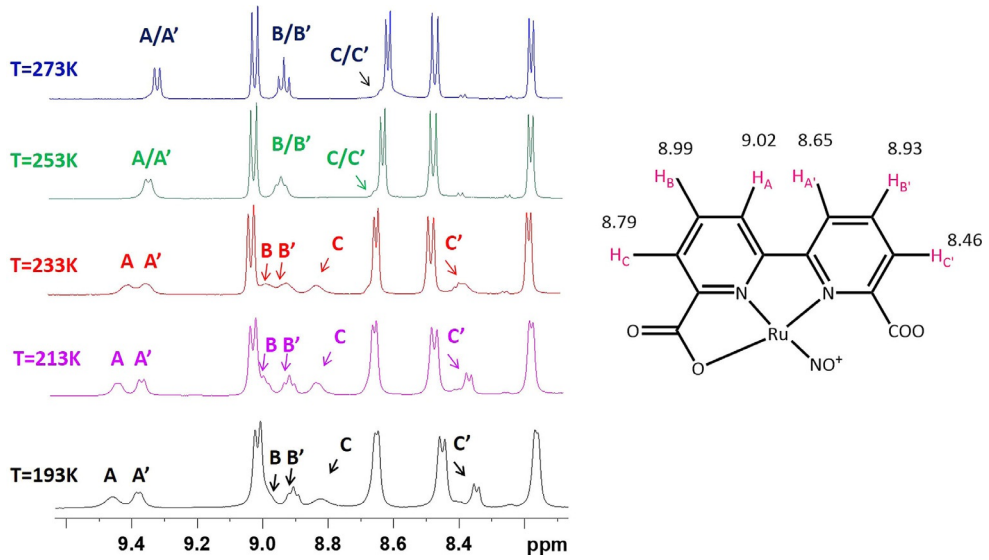

Figure 4. Left: VT ^{1}H NMR spectra for $\mathbf{2}^{3+}$ in [D_6]acetone. Right: computed chemical shifts at the M06 level of theory for the bda^{2-} protons in $\mathbf{2}^{3+}$. See Scheme 1 for labeling.

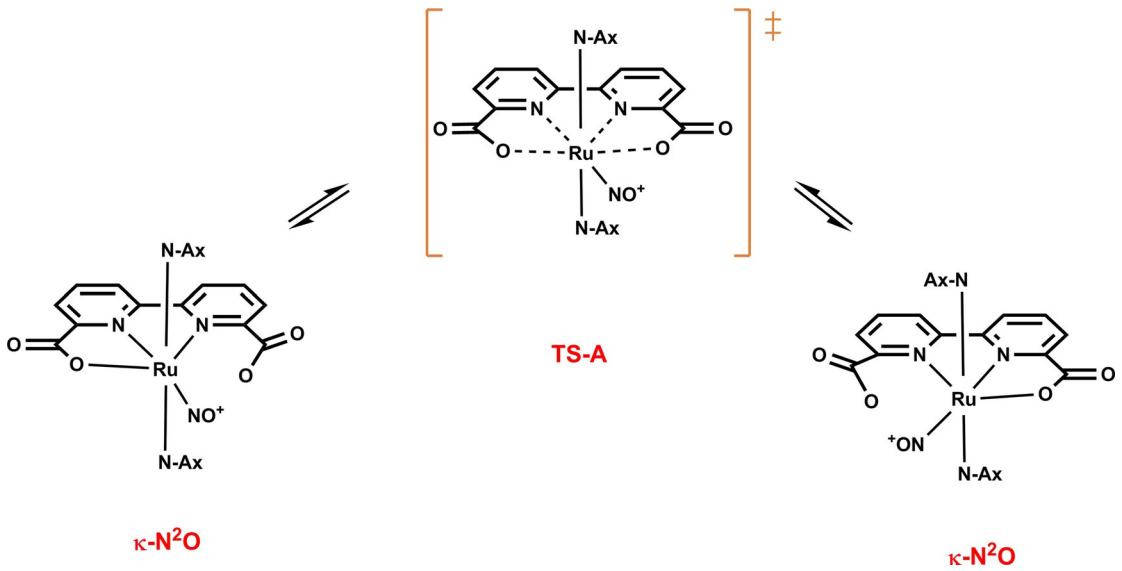

Scheme 3. Species involved in the fast equilibria associated with the dynamic behavior of $\mathbf{2}^{3+}$. Dashed lines indicate the bonds that are simultaneously formed and broken in the transition state TS-A. The DFT calculated structure for this complex is depicted in Figure 3, right.

$\mathbf{NO^2(H_2O)_4}]^{2+}$, the most unusual distances are the Ru–N distances of 2.26 and 2.82 Å, which are respectively 0.1 and 0.7 Å longer than the typical Ru–N bonds for related complexes. The computed chemical shifts at the M06 level of theory for the optimized structures (Figure S25 in the Supporting Information) are consistent not with those of the $[\mathbf{4}$-κ-$\mathbf{N^2O(H_2O)_4}]^{2+}$ isomer (Path A, Scheme 4) or those of $[\mathbf{4}$-κ-$\mathbf{NO^2(H_2O)_4}]^{2+}$ (Path B, Scheme 4), but with those of a mixture of both of them. The combination of all these equilibria is depicted in Scheme 4 (Paths A, B, and C), in which explicit water molecules are not shown for the sake of simplicity.

The isomers of the one-electron oxidized complex, $[\mathbf{5}$-κ-$\mathbf{N^2O(H_2O)_4}]^{3+}$ and $[\mathbf{5}$-κ-$\mathbf{NO^2(H_2O)_4}]^{3+}$, were also optimized at the M06 level of theory, and the corresponding structures and most relevant geometric parameters are presented in Figure 6 and Table 1. For the one-electron oxidized isomers, the bond lengths of the first and second coordination spheres are shortened compared to those found for the $\mathbf{4}^{2+}$ counterparts, as expected.[37] However, the most relevant distances for both isomers (Ru–N 2.46 Å for $[\mathbf{5}$-κ-$\mathbf{NO^2(H_2O)_4}]^{3+}$ and Ru–O 3.06 Å for the dangling carboxylate group in $[\mathbf{5}$-κ-$\mathbf{N^2O(H_2O)_4}]^{2+}$) remain comparable to those of its related complex in oxidation state II.

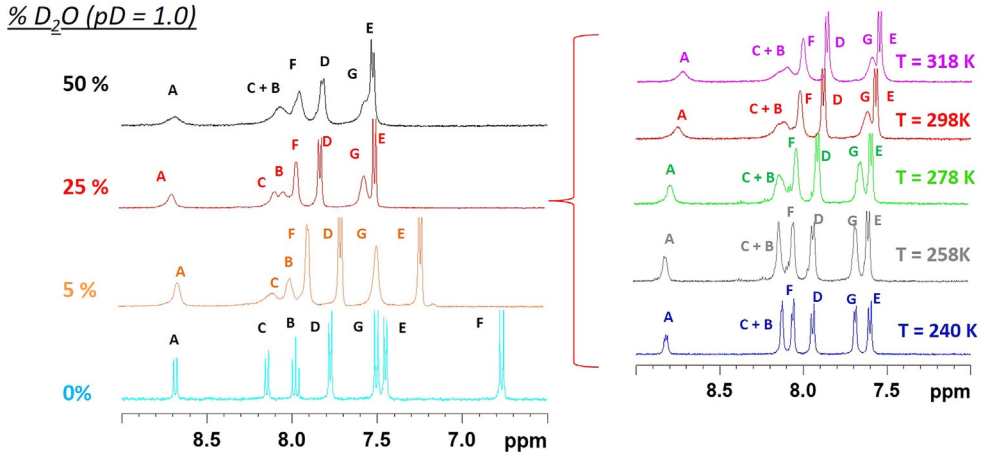

Figure 5. Left: ^{1}H NMR spectra of **1** in [D$_4$]MeOH (cyan spectrum) and of $\mathbf{4}^{2+}$ with different amounts of a solution of 0.1 M CF_3SO_3D in D_2O (labeled as D_2O, pD = 1.0) at 298 K. Right: VT ^{1}H NMR spectra of $\mathbf{4}^{2+}$ in [D$_4$]MeOH with 25% D_2O, pD = 1.0. Samples were prepared under rigorous N_2 atmosphere. See Scheme 1 for labeling.

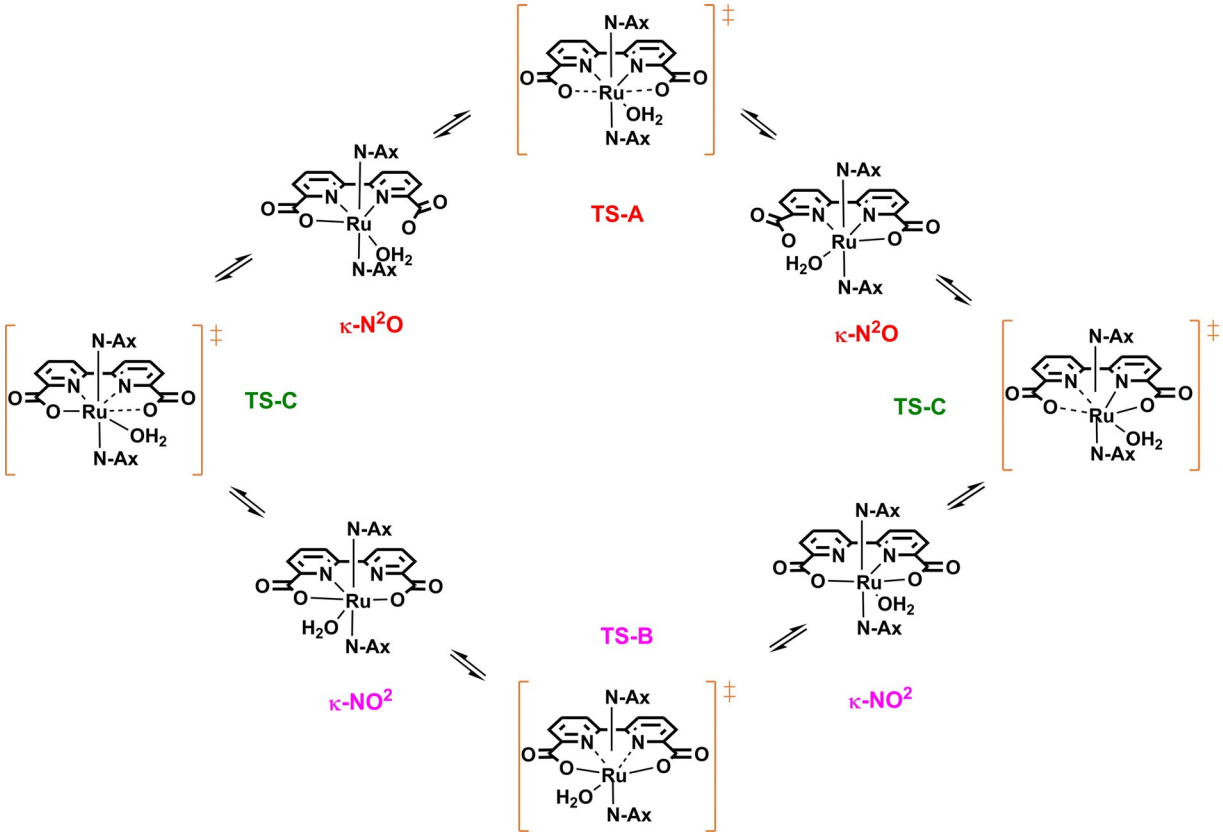

Scheme 4. Reaction pathways leading to a combination of equilibria involved in the dynamic behavior of $\mathbf{4}^{2+}$ or $\mathbf{5}^{3+}$ in acidic aqueous solution. The dashed lines indicate bonds that are simultaneously formed and broken in the transition states. Water molecules of solvation are omitted for clarity. Three different pathways A–C are identified depending on the transition state through which the species are interconverted.

Another interesting feature of these complexes is their relative energies. Whereas in oxidation state II, the $[\mathbf{4}\text{-}\kappa\text{-}N^2O(H_2O)_4]^{2+}$ isomer is favored by 20.3 kcal mol^{-1} with regard to the $[\mathbf{4}\text{-}\kappa\text{-}NO^2(H_2O)_4]^{2+}$ isomer, in oxidation state III this difference is drastically reduced to only 2.1 kcal mol^{-1}. While the energy comparison is only qualitative, because of the possibility of several conformers associated with solvent molecules hampering a reliable comparison, the trend is certainly significant.

To extract further experimental evidence about the potential combination of equilibria acting in the Ru(aqua) complexes bearing the bda^{2-} ligand in aqueous solution, we carried out XAS on frozen solutions of $\mathbf{5}^{3+}$. The results obtained are shown in Figure 2 and Table 1 together with those of **1**,

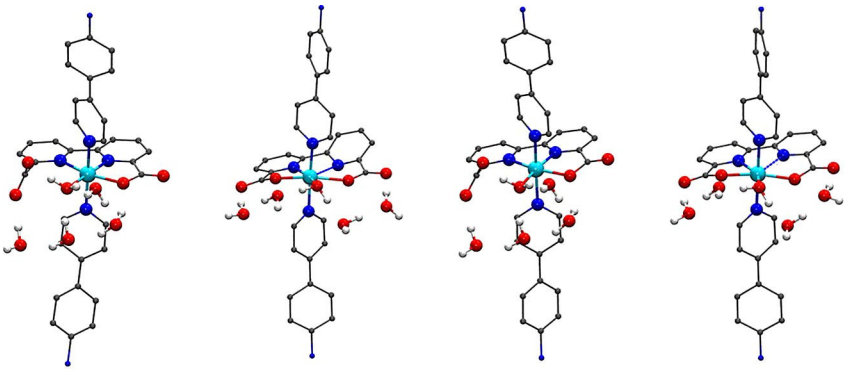

Figure 6. Ball-and-stick representations of the optimized structures of $[4\text{-}\kappa\text{-}N^2O(H_2O)_4]^{2+}$, $[4\text{-}\kappa\text{-}NO^2(H_2O)_4]^{2+}$, $[5\text{-}\kappa\text{-}N^2O(H_2O)_4]^{3+}$, and $[5\text{-}\kappa\text{-}NO^2(H_2O)_4]^{3+}$ at the M06 level of theory. Dashed lines indicate elongated bonds. Color code: Ru, cyan; C, gray; N, blue; O, red; H atoms of the ligands were omitted for clarity.

$[Ru^{III}Cl_3(trpy)]$ (trpy = 2,2′:6′,2″-terpyridine) and $Ru^{IV}O_2$, which were used as reference materials.

Table 1 lists the metric parameters $\mathbf{5}^{3+}$, extracted from EXAFS simulations (Figure 2 B). The EXAFS spectral changes for $\mathbf{5}^{3+}$ compared to **1** involve an overall shortening of the Ru–N/O bond lengths, leading to homogenization of the Ru–ligand distances in the first coordination sphere. Notably, a distance of about 2.54 Å that improves the quality of the EXAFS fit by a factor of about two was detected (Table S1 in the Supporting Information). This additional distance is thus indicative that $[5\text{-}\kappa\text{-}NO^2(H_2O)_n]^{3+}$ is present in the mixture of isomers in this oxidation state. In addition, the metric parameters obtained from EXAFS coincide well with those obtained from the computed structures for $[5\text{-}\kappa\text{-}NO^2(H_2O)_4]^{3+}$, and this confirms the presence of these species in frozen aqueous solution (Table 1).

To the best of our knowledge, this is the first experimental demonstration that the **κ-NO²** coordination mode of the bda^{2-} ligand is relevant in the combination of potential isomers involved in Ru-bda-type complexes in low oxidation states, although it had been suggested on the basis of DFT calculations.[26] In addition, we also found a similar distance for the $[Ru(tda)(py)_2]$ catalyst precursor in oxidation state III, in which the two isomers, $[Ru^{III}(tda\text{-}\kappa\text{-}N^2O^2)(py)_2]^+$ and $[Ru^{III}(tda\text{-}\kappa\text{-}N^3O)(py)_2]^+$ coexist in the crystal structure.[13]

This counterintuitive behavior of the coordination modes of bda^{2-} in $\mathbf{4}^{2+}$ and $\mathbf{5}^{3+}$, which is different from that of their homologues $\mathbf{2}^{3+}$ and **3** in organic solvents, is mainly associated with the strong hydrogen-bonding belt among the aqua and carboxylate ligands, which provides the driving force to push away the bpy part of the bda^{2-} ligand with decoordination of one of the N atoms.[26]

Conclusions

Our results based on VT NMR and XAS data as well as DFT calculations provide a detailed description of the nature of the species involved in the catalysis of water oxidation by Ru-bda-type complexes in low oxidation states, in which the critical Ru(aqua) moiety that provides access to the catalytic cycle is formed. The results show the fundamental need for a flexible and adaptable ligand, such as bda^{2-}, both from an electronic and geometrical perspective, to comply with the demands of the Ru centers in the different oxidation states. Further, for the first time we have shown experimentally the presence of isomers in Ru-bda-type complexes in which the ligand binds in a **κ-NO²** fashion.

Experimental Section

For synthetic procedures, X-ray crystallographic data in CIF format, and additional experimental, spectroscopic, electrochemical, and computational data, see the Supporting Information. CCDC 1014176 (**1**) and 1014177 ($\mathbf{2}^{3+}$) contain the supplementary crystallographic data for this paper. These data are provided free of charge by The Cambridge Crystallographic Data Centre.

Acknowledgments

A.L. and X.S. acknowledge MINECO/FEDER (CTQ2016-80058-R, CTQ2015-64261-R, CTQ-2015-73028-EXP, SEV 2013-0319, ENE2016-82025-REDT, CTQ2016-81923-REDC) and AGAUR (2017-SGR-1631) for financial support. R.M. and A.G. thank "La Caixa" foundation and MINECO (BES-2015-073069), respectively, for Ph.D. grants. M.H. thanks the Deutsche Forschungsgemeinschaft for financial support (grant Ha3265/6-1) and for a Heisenberg Fellowship and the German Bundesministerium für Bildung und Forschung for funding within the Röntgen–Ångström Cluster (grant 05K14KE1). We thank S. Reschke and M. Görlin for help in XAS data collection and M. Nachtegaal at SuperXAS of SLS for excellent technical support. The work at Brookhaven National Laboratory (M.Z.E.) was carried out under contract DE-SC0012704 with the US Department of Energy, Office of Science, Office of Basic Energy Sciences, and utilized resources at the BNL Center for Functional Nanomaterials. V.S.B. acknowledges financial support as part of the Argonne–Northwestern Solar Energy Research (ANSER) Center, an Energy Frontier Research Center funded by the US Department of

Energy, Office of Science, Office of Basic Energy Sciences under Award Number DE-SC0001059.

Conflict of interest

The authors declare no conflict of interest.

Keywords: coordination modes · N ligands · N,O ligands · ruthenium · water-oxidation catalysts

[1] S. W. Gersten, G. J. Samuels, T. J. Meyer, *J. Am. Chem. Soc.* **1982**, *104*, 4029 – 4030.
[2] P. Garrido-Barros, C. Gimbert-Suriñach, R. Matheu, X. Sala, A. Llobet, *Chem. Soc. Rev.* **2017**, *46*, 6088 – 6098.
[3] I. López, M. Z. Ertem, S. Maji, J. Benet-Buchholz, A. Keidel, U. Kuhlmann, P. Hildebrandt, C. J. Cramer, V. S. Batista, A. Llobet, *Angew. Chem. Int. Ed.* **2014**, *53*, 205 – 209; *Angew. Chem.* **2014**, *126*, 209 – 213.
[4] J. Creus, R. Matheu, I. Peñafiel, D. Moonshiram, P. Blondeau, J. Benet-Buchholz, J. García-Antón, X. Sala, C. Godard, A. Llobet, *Angew. Chem. Int. Ed.* **2016**, *55*, 15382 – 15386; *Angew. Chem.* **2016**, *128*, 15608 – 15612.
[5] R. Matheu, I. A. Moreno-Hernandez, X. Sala, H. B. Gray, B. S. Brunschwig, A. Llobet, N. S. Lewis, *J. Am. Chem. Soc.* **2017**, *139*, 11345 – 11348.
[6] L. Duan, F. Bozoglian, S. Mandal, B. Stewart, T. Privalov, A. Llobet, L. Sun, *Nat. Chem.* **2012**, *4*, 418 – 423.
[7] C. J. Richmond, R. Matheu, A. Poater, L. Falivene, J. Benet-Buchholz, X. Sala, L. Cavallo, A. Llobet, *Chem. Eur. J.* **2014**, *20*, 17282 – 17286.
[8] L. Wang, L. Duan, Y. Wang, M. S. G. Ahlquist, L. Sun, *Chem. Commun.* **2014**, *50*, 12947 – 12950.
[9] M. Schulze, V. Kunz, P. D. Frischmann, F. Würthner, *Nat. Chem.* **2016**, *8*, 576 – 583.
[10] F. Li, B. Zhang, X. Li, Y. Jiang, L. Chen, Y. Li, L. Sun, *Angew. Chem. Int. Ed.* **2011**, *50*, 12276 – 12279; *Angew. Chem.* **2011**, *123*, 12484 – 12487.
[11] H. Dau, M. Haumann, *Biochim. Biophys. Acta* **2007**, *1767*, 472 – 483.
[12] N. Cox, M. Retegan, F. Neese, D. A. Pantazis, A. Boussac, W. Lubitz, *Science* **2014**, *345*, 804 – 808.
[13] R. Matheu, M. Z. Ertem, J. Benet-Buchholz, E. Coronado, V. S. Batista, X. Sala, A. Llobet, *J. Am. Chem. Soc.* **2015**, *137*, 10786 – 10795.
[14] R. Matheu, M. Z. Ertem, M. Pipelier, J. Lebreton, D. Dubreuil, J. Benet-Buchholz, X. Sala, A. Tessier, A. Llobet, *ACS Catal.* **2018**, *8*, 2039 – 2048.
[15] L. Duan, L. Wang, F. Li, F. Li, L. Sun, *Acc. Chem. Res.* **2015**, *48*, 2084 – 2096.
[16] L. Duan, L. Wang, F. A. K. Inge, A. Fischer, X. Zou, L. Sun, *Inorg. Chem.* **2013**, *52*, 7844 – 7852.
[17] R. Matheu, L. Francàs, P. Chernev, M. Z. Ertem, V. S. Batista, M. Haumann, X. Sala, A. Llobet, *ACS Catal.* **2015**, *5*, 3422 – 3429.
[18] Y. Gao, X. Ding, J. Liu, L. Wang, Z. Lu, L. Li, L. Sun, *J. Am. Chem. Soc.* **2013**, *135*, 4219 – 4222.
[19] L. Duan, C. M Araujo, M. S. G. Ahlquist, L Sun, *Proc. Natl. Acad. Sci. U. S. A.* **2012**, *109*, 15584 – 15588.
[20] J. J. Concepcion, D. K. Zhong, D. J. Szalda, J. T. Muckerman, E. Fujita, *Chem. Commun.* **2015**, *51*, 4105 – 4108.
[21] M. V. Sheridan, B. D. Sherman, R. L. Coppo, D. Wang, S. L. Marquard, K.-R. Wee, N. Y. Murakami Iha, T. J. Meyer, *ACS Energy Lett.* **2016**, *1*, 231 – 236.
[22] X. Sala, S. Maji, R. Bofill, J. García-Antón, L. Escriche, A. Llobet, *Acc. Chem. Res.* **2014**, *47*, 504 – 516.
[23] Q. Daniel, P. Huang, T. Fan, Y. Wang, L. Duan, L. Wang, F. Li, Z. Rinkevicius, F. Mamedov, M. S. G. Ahlquist, S. Styring, L. Sun, *Coord. Chem. Rev.* **2017**, *346*, 206 – 215.
[24] L. Duan, A. Fischer, Y. Xu, L. Sun, *J. Am. Chem. Soc.* **2009**, *131*, 10397 – 10399.
[25] P. Pyykkö, *J. Organomet. Chem.* **2006**, *691*, 4336 – 4340.
[26] J. Nyhlén, L. Duan, B. Åkermark, L. Sun, T. Privalov, *Angew. Chem. Int. Ed.* **2010**, *49*, 1773 – 1777; *Angew. Chem.* **2010**, *122*, 1817 – 1821.
[27] D. W. Stephan, *Comprehensive Inorganic Chemistry II*, 2nd ed (Eds.: J. Reedijk, K. Poeppelmeier), Elsevier, Oxford, **2013**.
[28] P. P. Samuel, K. C. Mondal, N. Amin Sk, H. W. Roesky, E. Carl, R. Neufeld, D. Stalke, S. Demeshko, F. Meyer, L. Ungur, L. F. Chibotaru, J. Christian, V. Ramachandran, J. van Tol, N. S. Dalal, *J. Am. Chem. Soc.* **2014**, *136*, 11964 – 11971.
[29] C. Di Giovanni, A. Poater, J. Benet-Buchholz, L. Cavallo, M. Sola, A. Llobet, *Chem. Eur. J.* **2014**, *20*, 3898 – 3902.
[30] I. Romero, M. Rodríguez, A. Llobet, M.-N. Collomb-Dunand-Sauthier, A. Deronzier, T. Parella, H. Stoeckli-Evans, *J. Chem. Soc. Dalton Trans.* **2000**, 1689 – 1694.
[31] C. Di Giovanni, L. Vaquer, X. Sala, J. Benet-Buchholz, A. Llobet, *Inorg. Chem.* **2013**, *52*, 4335 – 4345.
[32] Y. Zhao, D. Truhlar, *Theor. Chem. Acc.* **2008**, *120*, 215 – 241.
[33] J. Pinson, F. Podvorica, *Chem. Soc. Rev.* **2005**, *34*, 429 – 439.
[34] L. Tong, L. Duan, Y. Xu, T. Privalov, L. Sun, *Angew. Chem. Int. Ed.* **2011**, *50*, 445 – 449; *Angew. Chem.* **2011**, *123*, 465 – 469.
[35] L. Alibabaei, B. D. Sherman, M. R. Norris, M. K. Brennaman, T. J. Meyer, *Proc. Natl. Acad. Sci. USA* **2015**, *112*, 5899 – 5902.
[36] R. G. Pearson, *J. Am. Chem. Soc.* **1963**, *85*, 3533 – 3539.
[37] H. C. Stynes, J. A. Ibers, *Inorg. Chem.* **1971**, *10*, 2304 – 2308.

Manuscript received: March 12, 2018
Revised manuscript received: June 6, 2018
Accepted manuscript online: June 13, 2018
Version of record online: August 20, 2018